Imaging from the Implantable Side: Ultrasonic-powered EIT System for Surgical Site Infection Detection

Bruno M. G. Rosa
The Hamlyn Centre
Imperial College London
London SW7 2AZ, UK
Email: b.gil-rosa@imperial.ac.uk

Guang Z. Yang
The Hamlyn Centre
Imperial College London
London SW7 2AZ, UK
Email: g.z.yang@imperial.ac.uk

***Abstract*—Ultrasounds are a proven medical tool to assess some biological processes, including breast cancer screening, foetal development and blood perfusion. However, ultrasounds also have the potential to deliver power and telemetry capabilities to deeply implant devices, surpassing some of the challenges faced by coils or antennas operating inside the human body. In this paper, we present a small-form implantable device activated by ultrasounds that can perform *in situ* tissue impedance imaging. The goal is to provide a diagnosis tool to evaluate soft tissue healing after surgery, by searching for areas of bacterial infection as the normal conductivity of tissue will be impaired, a phenomena undetected by standard imaging methods. The benefits that can come from this technology are the reduction of the morbidity rate associated with wound infections and recovery time for patients in hospital. The results obtained by the device have already shown a good performance in tracking conductivity perturbations in two-dimensional domains as part of the experimental setup devised for impedance measurements.**

I. Introduction

Ultrasounds (US) have been extensively used in medicine for imaging and therapeutic applications using the interaction between the sound waves and the tissues in the transmission path, mediated by the acoustic impedance [1]. The vast majority of these interactions occur in a *passive* way in which the acoustic beam do not interfere with the normal functioning of the biological tissues nor trigger any physiological event. In recent years, research on miniaturized implantable devices is attempting to employ US to deliver both power and telemetric capabilities to the devices transcutaneously, as an alternative to the magnetic and radiofrequency links [2], [3], [4]. The design of such devices include not only the last developments in MEMS technology but also employ smart materials in the form of film bulk acoustic and surface wave resonators for remote biosensing and actuation [5].

In a different direction, the so-called Electrical Impedance Tomography (EIT) is an emerging imaging modality that aims to reconstruct the internal conductivity distribution of a tissue from voltage measurements taken at the boundary [6]. It can be regarded as an extension of the bioimpedance method, where a set of boundary electrodes are responsible for the injection of a current that flows internally, producing surface potentials as a consequence of the tissue's behaviour under electrical stimuli. The process repeats itself for different current injection patterns and voltage recording locations in order to complete a tomographic frame acquisition.

Thus far, EIT has never been proposed as an untethered application where electrodes are in direct contact with the internal organs of the human body. The difference in conductivity among internal tissues is the basis for their identification within the tomographic slices [7] and any alteration to the functioning and/or physiological state will induce EIT variations. As examples, cancer and bacterial infection [8] exhibit different electrical response as compared to the normal healthy tissue. So, it is the objective of this paper to combine the penetration depth of ultrasounds with the imaging capability of EIT into a single device for tissue healing monitoring after surgery, as Fig. 1 suggests. This is a major healthcare burden since the morbidity rate associated with wound infection accounts for 1/3 of the postoperative deaths, while patients remaining in hospital for extended periods have a 5% risk of developing a new infection [9].

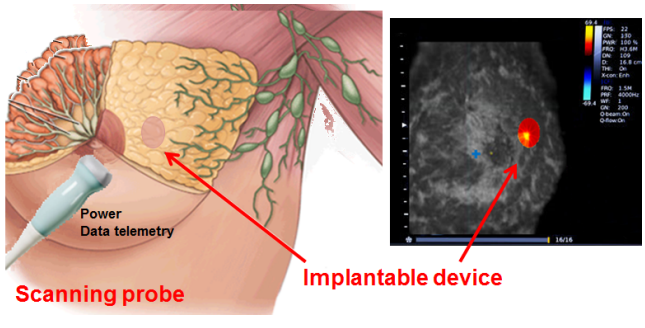

Fig. 1: The futuristic concept behind the ultrasonic-powered EIT system developed for tissue impedance imaging at the implant side. A battery-less device with conformal shape is kept at the surgical site to assess tissue healing over time. Non-continuous monitoring of the site by an ultrasonic scanning probe will provide anatomical information combined with functional data retrieved by EIT.

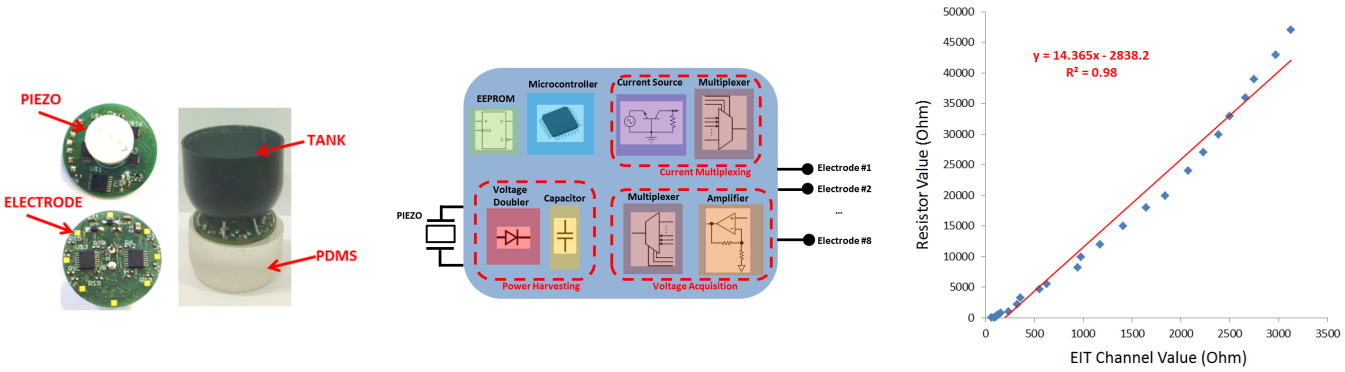

(a) (b) (c)

Fig. 2: Ultrasonic-powered EIT device for tissue impedance imaging. **a)** Top and bottom layers of the circuit board ($\varnothing$ = 2 cm) with experimental tank for conductivity evaluation. **b)** Diagram of the electronic modules composing the device. **c)** Response of the device as a function of the resistance value (real part of impedance) obtained for some discrete resistors, using single channel acquisition.

II. Material and Methods

This section details the electronic design of the implantable device and the mathematical formulation applied to EIT in terms of the Forward and Inverse Problems. Some performance results are also provided in each subsection, while the assessment of the imaging modality as a whole is given in the *Results* section, by using the measurements obtained by the device as the input data to the reconstruction algorithm.

A. Electronic Design

The proposed device is shown in Fig. 2a and resorts to ultrasound scavenging to power-up device electronics. The acoustic wave is produced externally by a PZT (MCUSD11A400 from *Multicorp*) excited in the harmonic regime with frequency of 400 kHz. Conversion from acoustic to electrical energy is performed by a similar piezo on the implant side and DC power is obtained after a voltage doubler rectifier connected to a large capacitor to hold the electrical charges, as depicted in Fig. 2b. The DC level powers all electronics with total current consumption close to 100 μA. This allows to operate the device at depths of 4 cm, where the harvested level hardly exceeds 0.8 V [10]. The control of the device is performed by a microcontroller (MSP430L092, *Texas Instruments*) and current switching through the eight available electrodes is performed by a signal multiplexer (TS4100, *Silicon Labs*). The amplitude for current excitation is set to 20 μA, a level within the safe physiological range registered for tissues [7]. By its turn, voltage measurements are performed using a non-inverting amplifier (TS1004, Silicon Labs) at each electrode, followed by digitalization in succession (TS4101, *Silicon Labs*) with 8-bit of resolution. The performance of the device is shown in Fig. 2c in terms of the resistance value (inverse of conductance) obtained when all the electrical current is flowing through discrete resistors.

The binary pattern from each voltage sample is coded using ON-OFF modulation (OOK) at the terminals of the implantable piezo, thereby modifying the acoustic transmission line seen by the external PZT which produces a detectable pattern over the same energy-carrying wave. Each complete data set (for a particular current pattern) is acquired and transmitted within 500 milliseconds, leading to a total scanning time of 4 s to swap between the 8 electrodes. The total number of voltage measurements available for the EIT system is then **8 x 8 = 64**, although only **(8 x 7)/2** are independent measurements, yielding 23 degrees-of-freedom for the image reconstruction procedure described below [11].

B. Forward Problem in EIT

The mathematical model for EIT is derived from Ampère's Law in Electromagnetism in the condition of electrostatics ($\nabla \times \overrightarrow{E} = 0$) and harmonic regime of excitation of the electric field, obtaining a simplified complex relation of the form,

$$\nabla \times \overrightarrow{H} = (\sigma + j\omega\epsilon)\overrightarrow{E} \tag{1}$$

where $\overrightarrow{H}$ is the magnetic field, $\overrightarrow{E}$ the electric field, σ the conductivity, ω the frequency and ϵ the permittivity. For the low frequency range employed in the imaging modality, $\omega \rightarrow 0$, which means that the conductivity of materials dominates over permittivity, and the latter can be dropped from the formulation. Applying the divergence operator in the left-hand side of last equation, one gets,

$$\nabla \cdot (\nabla \times \overrightarrow{H}) = 0 \implies \nabla \cdot \sigma \overrightarrow{E} = 0 \tag{2}$$

with the annulment arising from the properties of the differential operators. The irrotational nature of $\overrightarrow{E}$ also implies that the field can be given by the gradient of a scalar potential ϕ, which completes the formulation for EIT in Eq. 3 [11].

$$\nabla \cdot \sigma \nabla \phi = 0 \tag{3}$$

In the boundary of the tissue, electrodes are the source and sink of the current and the magnitude of the electrical potential over these elements must be included in last expression ($\phi^{in}_{boundary} = -\phi^{out}_{boundary}$). Finally, the resolution of Eq. 3 in terms of ϕ for a particular distribution σ constitutes

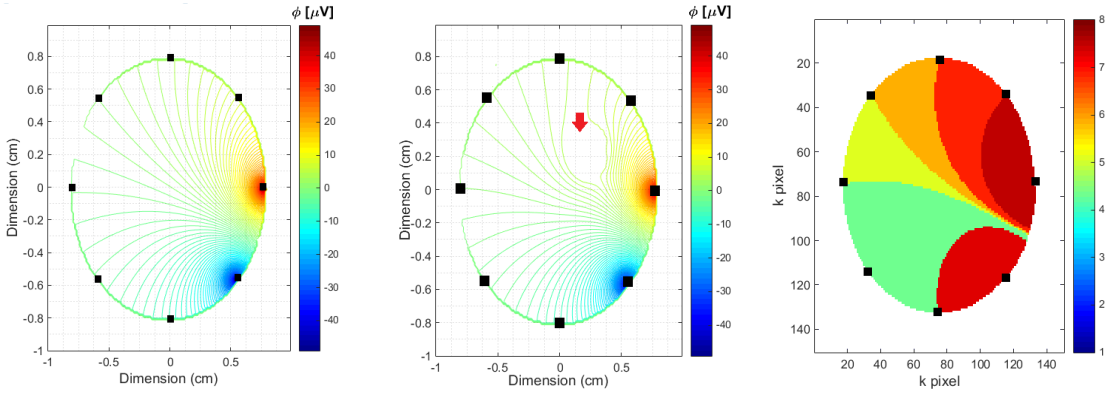

(a) (b) (c)

Fig. 3: Numerical simulations obtained for the EIT domain in two-dimensions, surrounded by the eight surface electrodes. **a)** Electrical potential distribution calculated for a background conductivity in the entire extension of the domain. **b)** Electrical potential distribution for a small conductivity perturbation in the background map, that disturbs the equipotential lines in the area pointed by the arrow. **c)** Back-projection operator obtained for a current dipole located in Quadrant IV, with image *pixels* assigned to the number of surface electrode projected by the transformation.

the Forward Problem and examples are provided in Fig. 3a and 3b using the same current dipole with different σ maps.

C. Inverse Problem in EIT

The inverse process constitutes the essence of any imaging modality, aiming to reconstruct the conductivity distribution map from the potentials (voltage samples) recorded at the boundary. However, due to the impossibility of sampling all boundary points and the errors involved in the measurement process itself, inversion of the EIT system is an *ill-posed* problem and so, it requires optimization techniques using either liner or non-linear approaches [12].

In this paper, we use a linear 2D back-projection algorithm based on the work of Santosa and Vogelius [13]. It consists in assigning to every *pixel* in the image domain the corresponding potential registered at the boundary, by following the electric field lines passing through the *pixel* location until they reach the boundary. It is a similar process to the Radon Transform employed in CT, but applied to curvilinear geometries. Seeing that the boundary cannot be covered in its entire extension by just 8 electrodes, some terminations of the field lines will not correspond to a valid electrode location and henceforth, the corresponding *pixel* will be assigned to the nearest electrode vale by the back-projection operator $\mathbb{P}_i$, in every rotation of the current dipole over the boundary, as depicted in Fig. 3c.

Whenever the data vectors containing the voltage samples acquired for the perturbed and background conductivity maps are available, the disturbed map is calculated from the background one as,

$$\delta\sigma_k + \sigma_k = -\frac{1}{m}\sum_{i=1}^{m}\frac{\mathbb{P}_i(\delta\sigma_k + \sigma_k)}{\mathbb{P}_i(\sigma_k)}\sigma_k \qquad (4)$$

where index k represents the *pixels* within the image and i the number of current dipole rotations (m = 8).

III. Results

The implantable device was tested using a calibrated conductivity solution (1413 μS/cm) inside a tank surrounded by 8 copper tape electrodes in equidistant positions attached to the walls of the container. Since we are performing two-dimensional reconstructions of the conductivity only, the level of the solution within the tank does not influence the measurements, as long as the eight electrodes remain completely covered by the solution. PDMS material was employed as the acoustic transmission medium between the implantable and external PZTs with a thickness of 2 cm. The latter PZT is fed with a signal derived from a waveform generator that produces the 400 kHz sine-wave. The OOK modulation is detected *via* a demodulator circuit tuned to the same frequency followed by a logic analyser to recover the binary patterns sent by the implantable device. Perturbations to the background conductivity (2600 μS/cm) with two different diameters were imposed in the same location within

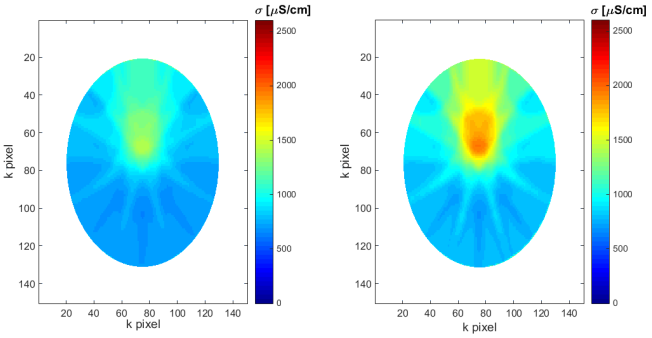

(a) (b)

Fig. 4: Conductivity reconstructions obtained for different diameters of the perturbation, located in the same position within the tank. **a)** ∅ = 0.25 cm. **b)** ∅ = 0.5 cm.

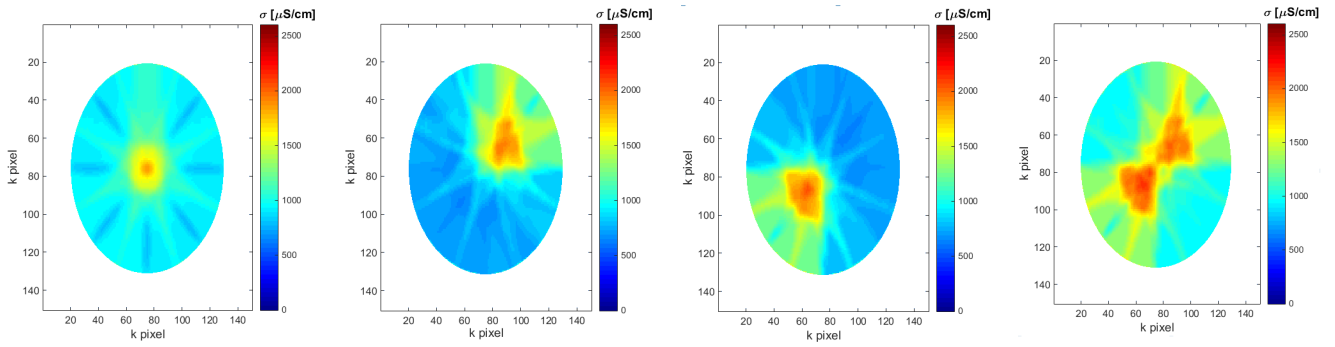

Fig. 5: Conductivity reconstructions obtained for different locations of the disturbance (∅ = 0.5 cm). **a)** Centre. **b)** Quadrant I. **c)** Quadrant III. **d)** Double perturbation in Quadrants I and III.

the tank, as presented in Fig. 4, and different positions of the perturbation in Fig. 5. After the back-projection routine, images were additionally filtered by a **5 x 5** gaussian mask to smooth-out the conductivity transitions between neighbour *pixels*, specially in the areas surrounding the electrodes.

IV. Discussion

The results obtained have shown a good performance of the imaging modality in tracking the correct location of the perturbation within the tank. However, the correct shape and contour of the disturbance - circle - was not completely achieved and a blurring effect in the areas laying between the disturbance and nearest electrodes still remains. Additionally, effects of the projections are also visible in the domain as a *star* artifact. These effects could have been attenuated by two processes: a different reconstruction scheme using non-linear methods to cope with the large discrepancy between domain size and the number of degrees-of-freedom yielded by the measurement process; and/or augmenting the number of device electrodes. The latter solution is impractical for implants as it implies increasing the physical size of the device and power consumption. Nonetheless, the proposed solution was still able to detect multiple disturbances within the tank, a fact of the utmost importance since, in a real scenario, bacteria tend to form colonies that disseminate all over the surgical site. Moreover, the magnitude registered for conductivity over time can provide an indication of the stage of development of such colonies as it changes with the diameter of the disturbance.

Finally, for the scenario where impedance values in the measurement process are outside the calibration curve of the device, the amplitude of the excitation current can be easily reset in order to accommodate the new range, as conductivity varies greatly among biological tissues and also in the physiological and pathological states [7].

V. Conclusion

An implantable device with ultrasonic power scavenging has been proposed that can detect conductivity perturbations in the structure of the domain and transmit that detection to the exterior of the body. As the size of PZTs and electronics continue to scale-down, in the future, it will be possible to conform the shape of the device to any tissue geometry or surgical patch, so as to provide proper enclosing of the scanned area. Flexible substrates that can support the electronics and hold the structure in place are also topics that require further research, to which this study constitutes a first attempt to achieve imaging directly over the implant.

Acknowledgment

The authors would like to thank to the Engineering and Physical Science Research Council for the financial support under the project grant "EPSRC EP/L014149/1".

References

[1] Szabo, T. L., *Diagnostic Ultrasound Imaging: Inside Out.* Elsevier, Inc., London, 2004.

[2] Bazaka, K. and Jacob, M. V., *Implantable Devices: Issues and Challenges.* Electronics, vol. 2, pp. 1 - 34, 2013.

[3] Ozeri, S. and Shmilovitz, D., *Ultrasonic transcutaneous energy transfer for powering implanted devices.* Ultrasonics, vol. 50, pp. 556 - 566, 2010.

[4] Seo, D. *et al*, *Wireless Recording in the Peripheral Nervous System with Ultrasonic Neural Dust.* Neuron, vol. 91, issue 3, pp. 529 - 539, 2016.

[5] Voiculescu, I. and Nordin, A. N., *Acoustic wave based MEMS devices for Biosensing applications.* Biosens Bioelectron, vol. 33, pp. 1 - 9, 2012.

[6] Bayford, R. H., *Bioimpedance tomography (electrical impedance tomography).* Annu Rev Biomed Eng, vol. 8, pp. 63-91, 2006.

[7] Grimnes, S. and Martinsen, O. G., *Bioimpedance and Bioelectricity Basics - $2^{n.d}$ Edition.* Elsevier Ltd., 2008.

[8] Ekhtelat, M., *Impediometric Technique as a Rapid Estimation to Detect Pathogenic Bacteria in Quality Control.* J Nat Pharm Prod, vol. 11, no. 2, 2016.

[9] *Surgical site infection, prevention of surgical site infection.* NICE Clinical Guidelines, no. 74, London, 2008.

[10] Rosa, B. and Yang, G. Z., *Active Implantable Sensor Powered by Ultrasounds With Application in the Monitoring of Physiological Parameters for Soft Tissue.* IEEE 13^{th} International Conference on Wearable and Implantable Body Sensor Networks, 2016.

[11] Seo, J. K. *et al*, *Magnetic resonance electrical impedance tomography (MREIT): conductivity and current density imaging.* J Phys Conf Ser, vol. 12, pp. 140 - 155, 2005.

[12] Vogel, C. R., *Computational Methods for Inverse Problems.* Society for Industrial and Applied Mathematics, 2002.

[13] Nan, P. C. *et al*, *An Implementation of the back-projection algorithm according to Santosa and Vogelius.* ABCM Symposium Series in Bioengineering, vol. 1, 2006.